Swansea University
Prifysgol Abertawe

Cronfa
Setting Research Free

Cronfa - Swansea University Open Access Repository

This is an author produced version of a paper published in :
RSC Adv.

Cronfa URL for this paper:
http://cronfa.swan.ac.uk/Record/cronfa20699

Paper:
Jin, L., Mei, J. & Li, L. (2014). Nonlinear dynamics of a doubly clamped carbon nanotube resonator considering surface stress. *RSC Adv., 5*(10), 7215-7221.

http://dx.doi.org/10.1039/c4ra08806a

This article is brought to you by Swansea University. Any person downloading material is agreeing to abide by the terms of the repository licence. Authors are personally responsible for adhering to publisher restrictions or conditions. When uploading content they are required to comply with their publisher agreement and the SHERPA RoMEO database to judge whether or not it is copyright safe to add this version of the paper to this repository.
http://www.swansea.ac.uk/iss/researchsupport/cronfa-support/

Nonlinear dynamics of doubly clamped carbon nanotube resonator considering surface stress

Leisheng Jin, Jie Mei, and Lijie Li

AUTHOR ADDRESS: Multidisciplinary Nanotechnology Centre, College of Engineering, Swansea University, Swansea, SA2 8PP, UK.

KEYWORDS: Doubly clamped carbon nanotube (CNT) resonators, Surface effect, Whirling, Chaotic motion, Accelerometer

ABSTRACT: Doubly clamped carbon nanotube (CNT) resonators have received much attention due to their large stiffness, low density and small cross-section, making them suitable as highly sensitive mass sensors and signal processing units. In this paper, new study on dynamic performance of such resonators taking account of the surface effect has been performed and interesting findings have been unveiled. It is found that the surface effect causes increased resonant frequency, the whirling and chaotic motions to appear at much higher driving forces. For the first time, the whirling motions for the centre point of the resonator in *Y-Z* plane are found to display various Lissajous loops under different driving conditions. Based on the nonlinear analysis, new application of the resonator on accelerometers has been postulated and analyzed.

1. Introduction

Nanoelectromechanical systems (NEMS) resonators have been investigated by many researchers both theoretically and experimentally [1-5] with variety of applications such as in ultrasensitive mass sensing [6], and magnetometers [7]. Carbon nanotube (CNT) is one of most important candidates to act as NEMS resonator due to its superior mechanical characteristics such as low effective mass, large stiffness and high mechanical quality factor [8]. In order to produce highly sensitive sensors, analysis of both linear and nonlinear dynamics of CNT resonators has been conducted previously. Wu et al. [9] reported the capacitive spring softening effect observed in single-walled carbon nanotube (SWCNT) resonators. Li et al. demonstrated the sensitivity of resonant frequency shifts by both the tube length and diameter of the CNT resonator [9]. Rueckes et al. [11] showed that a suspended CNT can be used as a memory device based on its nonlinear pull-in behavior. Very recently, in reference [6], the authors proposed a nonlinear optical mass sensor based on a doubly clamped suspended CNT resonator in all-optical domain. A CNT resonator used to probe a very small anisotropic magnetic moment carried by nano-object in the magnetic hysteresis loop has been reported in [7].

So far, several research groups have employed the continuum mechanics model, i.e. elastic beam model [12] [7] [13] in modeling the dynamics of a NEMS resonator. In reference [14], Conley et al. developed a nonlinear elastic beam model for an electrostatically or magnetomotively excited nanotube resonator. Based on this model, an analytical criterion for the onset of the nonlinear jump phenomena and the nonplanar, whirling motions has been derived. Inspired by this work, Chen et al. [15] carried a detailed bifurcation analysis for electrostatically driven silicon nanowire resonators and concluded that the extensive chaotic motion is expected as the excitation magnitude increases to such an extent. However in that model, the surface effect

that should play a significant role in NEMS resonators, especially for a resonator whose transverse dimension (i.e. diameter) is smaller than sub-50 nm was neglected. Therefore, it naturally leads to a question as to how the surface effect plays its role in determining the nonlinear behavior of the NEMS resonators described in [15] [16]. The surface effect, which arises from the imbalance between the coordination numbers of the bulk atom and surface atom for a nanoscale resonator, has been thoroughly studied, and it is one of key parameters that determines the resonance of the nanostructures [12][17]. However, there is a lack of attention of studying its impact when resonators are vibrating in nonlinear regime. The nanoresonators working in nonlinear regimes have been proven to have high sensitivity in mass detection [18] and can be used to improve the measurement precision of resonant frequency [19]. Hence investigation of the surface effect of nanoresonator in nonlinear regimes is critically important. In this work, we focus on investigating how the surface effect determines the nonlinear behavior of a CNT resonator such as jump phenomena, whirling motion and chaotic vibration. Numerically, a partial differential equation is used to study the dynamics of a doubly –clamped nanotube resonator. It is found that surface effect can effectively change the onset of the nonlinear behavior, as well as the dynamical states. The detailed motion of the centre point of the resonator in *Y-Z* plane will also be investigated. An application of the resonator has been postulated and analyzed.

2. Model construction

The SWCNT resonator can be modeled as a clamped-clamped cylinder that is suspended above a trench, as shown in Figure 1. It is vibrating under an alternate electrostatic force applied from the bottom electrode. In the model, the initial distance between the bottom electrode and nanotube is h. The length, diameter, and wall thickness of the SWCNT are L, d and b

respectively. Under the electrostatic driving force, the nanotube oscillates in the similar manner as a doubly clamped, one dimensional mechanical beam. The surface effect should be considered as the resonator has large surface-to-volume ratio. Euler-Lagrange equation is used to derive the dynamical model. First, the initial surface stress can be represented by: $\tilde{\tau}_{xx} = \tau_0 + E_s \tilde{\varepsilon}_{xx}^s$, where τ_0 is the surface stress at zero strain. $\tilde{\varepsilon}_{xx}^s$ is the initial surface strain in the relaxed state. E_s is surface elastic modulus. As shown in Figure 1b, the red arrow represents the surface stress and the blue arrow represents bulk stress of the CNT during vibration. The two stresses are described as [20] $\tau_{xx}^t = \tilde{\tau}_{xx} + E_s e_{xx}^s$ (surface) and $\sigma_{xx}^t = \tilde{\sigma}_{xx} + E e_{xx}^s$ (bulk). Similar to Young's modulus E, E_s is a measure of stiffness of an elastic material surface, which is defined as the ratio of the stress on the surface to the strain. It is assumed that the surface stress is linearly proportional to the Green-Lagrangian stain e_{xx} ($e_{xx} = -z\frac{\partial^2 Z(x,t)}{\partial x^2} + \frac{1}{2}\left(z\frac{\partial^2 Z(x,t)}{\partial x^2}\right)^2 + \frac{1}{2}\left(\frac{\partial Z(x,t)}{\partial x}\right)^2$). Therefore the surface strain energy per unit volume W_s is described as:

$$W_s = \int \tau_{xx}^t de_{xx}^s = (\tilde{\tau}_{xx} + \frac{1}{2} E_s e_{xx}^s) e_{xx}^s \qquad (1)$$

Assuming $e_{xx}^s = e_{xx}$ at the surface of the tube, the incremental potential energy ΔU_1 which due to the internal force over the cross section and the surface effect is obtained by:

$$\Delta U_1 = \frac{1}{2}[EI_m + \tilde{\tau}_{xx} I_s + E_s I_s](\frac{\partial^2 Z}{\partial x^2})^2 + \frac{1}{2}\tilde{\tau}_{xx} C(\frac{\partial Z}{\partial x^2})^2 \qquad (2)$$

where C is the circumference. I_m and I_s are the inertia moment and the surface inertia moment respectively. E is the Young's modulus. The incremental potential energy ΔU_2 due to bending induced tension and kinetic energy T per unit length of the resonator can be expressed as follows:

$$\Delta U_2 == \frac{1}{2}\left\{\frac{EA}{2L}\int_0^L [(\frac{\partial Z}{\partial x})^2 + (\frac{\partial Y}{\partial x})^2]dx\right\}(\frac{\partial Z}{\partial x})^2 \qquad (3)$$

$$T = \frac{1}{2}\rho A(\frac{\partial Z}{\partial t})^2 \qquad (4)$$

where ρ is the density of the CNT. A is the cross-section area. $Y(x,t)$ is the displacement in Y-direction. Combining equations (2), (3) and (4), we can get the Euler-lagrange equation for the beam as:

$$S = \int_0^L \left[\frac{1}{2}\rho A(\frac{\partial Z}{\partial t})^2 - \frac{1}{2}[EI_m + \tilde{\tau}_{xx}I_s + E_sI_s](\frac{\partial^2 Z}{\partial x^2})^2 - (\tilde{\tau}_{xx}C + \frac{EA}{2L}\int_0^L [(\frac{\partial Z}{\partial x})^2 + (\frac{\partial Y}{\partial x})^2]dx)(\frac{\partial Z}{\partial x})^2\right]dx$$

(5)

The Lagrangian (L_a) is obtained as

$$L_a = \frac{1}{2}\rho A(\frac{\partial Z}{\partial t})^2 - \frac{1}{2}[EI_m + \tilde{\tau}_{xx}I_s + E_sI_s](\frac{\partial^2 Z}{\partial x^2})^2 - \frac{1}{2}(\tilde{\tau}_{xx}C + \frac{EA}{2L}\int_0^L [(\frac{\partial Z}{\partial x})^2 + (\frac{\partial Y}{\partial x})^2]dx)(\frac{\partial Z}{\partial x})^2 \qquad (6)$$

Equation (6) is then substituted into the following equation

$$\frac{\partial L_a}{\partial Z} - \frac{\partial}{\partial t}(\frac{\partial L_a}{\partial \dot{Z}}) - \frac{\partial}{\partial x}(\frac{\partial L_a}{\partial Z_x}) + \frac{\partial^2}{\partial x^2}(\frac{\partial L_a}{\partial Z_{xx}}) = 0 \qquad (7)$$

Since $\partial L_a / \partial Z = 0$, $\partial L_a / \partial \dot{Z} = \rho A \partial Z / \partial t$, $\partial L_a / \partial Z_x = -(\tilde{\tau}_{xx}C + \int_0^L [(\partial Z/\partial x)^2 + (\partial Y/\partial x)^2]dx)\partial Z/\partial x$.

We can have the dynamical equation in Z-direction considering as

$$[EI_m + \tilde{\tau}_{xx}I_s + E_sI_s]\frac{\partial^4 Z}{\partial x^4} - (\tilde{\tau}_{xx}C + \frac{EA}{2L}\int_o^L [(\frac{\partial Z}{\partial x})^2 + (\frac{\partial Y}{\partial x})^2]dx)\frac{\partial^2 Z}{\partial x^2} + \rho A\frac{\partial^2 Z}{\partial t^2} = F_e + F_f^Z \quad (8)$$

Similarly, following the same procedure, we can have the dynamical equation in Y-direction

$$[EI_m + \tilde{\tau}_{xx} I_s + E_s I_s]\frac{\partial^4 Y}{\partial x^4} - (\tilde{\tau}_{xx} C + \frac{EA}{2L}\int_o^L [(\frac{\partial Z}{\partial x})^2 + (\frac{\partial Y}{\partial x})^2]dx)\frac{\partial^2 Y}{\partial x^2} + \rho A \frac{\partial^2 Y}{\partial t^2} = F_f^Y \qquad (9)$$

Note that we have added the applied electrostatic force F_e and viscous damping force $F_f^{\{Y,Z\}}$ into equations (8) and (9). If the surface effect in equations (8) and (9) is ignored, they will be the same as those used in [14, 15]. In this work, will be used to study the deformations in Z and Y direction of the device. In equations (8) and (9), $I_m = \pi/4(d^4/16-(d/2-b)^4)$, $I_s = \pi/4(d^3/8-(d/2-b)^3)$. $A = \pi b(d-b)$, and $C = 2\pi d - 2\pi b$. The formulas of the two forces F_e, $F_f^{\{Y,Z\}}$ have been derived in [15],

$$F_e = -\frac{\pi\varepsilon_0 V^2(t)}{(Z+h)[\ln(4\frac{Z+h}{d})]^2} \approx -\frac{2\pi\varepsilon_0 (V_{dc}V_0)\cos(\omega t)}{h[\ln\frac{4h}{d}]^2} \qquad (10)$$

$$F_f^{\{Y,Z\}} = -\frac{\pi P d}{4v_T}\partial_t\{Y,Z\} \qquad (11)$$

In equation (10), the applied potential is $V = V_{dc} + V_{ac}\cos(\omega_d t + \phi)$, where V_{dc} and V_{ac} are dc and ac components of the potential with the drive frequency ω_d. It should be noted that the vibration in Z direction is much smaller compared with the gap h. Thus, we have the approximation in equation (10). In equation (11), $v_T = \sqrt{k_B T_k / m}$ is the air molecule velocity at T_k, where P and T_k are the air pressure and temperature respectively. k_B is the Boltzmann constant and m is molecular mass of air. In order to study the dynamic behavior of the resonator, we have employed Galerkin's method [21] which assumes that the $Z(x,t) = z(t)\varphi(x)$, $z(t)$ and $\varphi(x)$ are the time-dependent amplitude and deflection eigenmode respectively. The $\varphi(x) = (2/3)^{1/2}[1-\cos(2\pi x/L)]$ [12] is assumed and it satisfies the boundary conditions: $\varphi(0) = \varphi(L) = \varphi''(0) = \varphi''(L) = 0$. According to the procedure of the Galerkin's method, we multiply the $\varphi(x)$ on both sides of the equation (1)

and then integrate it by parts, the following dynamic equations that describe the defection of the device in Z and Y direction are obtained.

$$\begin{aligned} &\ddot{z} + \omega_0^2 z + az(z^2 + y^2) + \beta\dot{z} = -2F_0 \cos(\omega t) \\ &\ddot{y} + \omega_0^2 y + ay(z^2 + y^2) + \beta\dot{y} = 0 \end{aligned} \tag{12}$$

where

$$\omega_0 = (2\pi / L)^2 \sqrt{(EI_m)^* / 3\rho A(1 + P^* L^2 / 4\pi^2 (EI_m)^*)} \tag{13}$$

in which $(EI_m)^* = EI_m + \tilde{\tau}_{xx} I_s + E_s I_s$ and $P^* = \tilde{\tau}_{xx} C$, $\beta = \pi P d / (4 v_T \rho A)$, $\alpha = E / 18\rho (2\pi / L)^4$ and $F_0 = (\sqrt{2/3} / \rho A)\pi\varepsilon_0 V_{dc} V_{ac} / (h(\ln(4h/d))^2)$. It is clear to see from the equations (8) and (9) that the surface effect, represented by I_s, E_s, $\tilde{\tau}_{xx}$, has changed the bending rigidity EI_m into $EI_m + \tilde{\tau}_{xx} + E_s I_s$. Subsequently, the equation (12) derived from equations (8) and (9) has displayed an increased resonator frequency, which is expressed as in equation (13).

3. Calculation and results analysis

Based on equation (12), we have calculated periodic solutions when the driving voltage is low, i.e. V_{dc} is fixed at 0.5V and V_{ac} is varied in a small interval. Other parameters have been taken as: L=100 nm, b=0.066 nm, d=0.548 nm, $\rho = 1350$ kg/m^3, E=5.5×10^{12} Pa, h=500 nm, k_B=1.38×10^{23}, $\varepsilon_0 = 8.85 \times 10^{-12}$ and m=5.6×10^{-26} kg [15, 17]. As shown in Figures 2a and 2b, the vibration amplitude of the resonator in Z and Y when driving frequency varying in the range of $0.9\omega_0$ to $1.2\omega_0$ under different driving voltage V_{ac} without considering surface effect (E_s = 0, $\tilde{\tau}_{xx} = 0$) has been calculated. It is shown in Figure 2a that the resonator is vibrating periodically and the jump behavior at $V_{ac} \approx$ 0.7 V is observed. As the V_{ac} is increasing, the gap of the jump is

getting wider. In Figure 2b, it is seen that the vibration amplitude in Y direction is comparable to vibration amplitude in Z until V_{ac} = 1.5 V which means that the whirling motion has appeared when the V_{ac} is above 1.5 V. For comparison, the calculated results shown in Figures 2c and 2d are counterparts of Figures 2a and 2b taking consideration of the surface effect, where E_s = 5.19 N/m and $\tilde{\tau}_{xx} = 0.05$ N/m [22] are used. It should be noted that the natural frequency ω_0 has increased to 4.59×10^{10} Hz due to the surface effect. With the surface effect, the vibration amplitudes of the resonator in Z and Y directions have been calculated by sweeping the driving frequency in the range of $0.9\omega_0$ to $1.2\omega_0$ under different driving voltage V_{ac}, and results are shown in Figures 2c and 2d. In Figure 2c, it is seen that the voltage V_{ac} at which the jump behavior occurs has increased to 1.5 V. Also the curves representing the relations between V_{ac} and ω get more condensed and sharper than Figure 2a. Likewise, it is noted that vibration amplitude in Y direction in Figure 2d is comparable with that in Z direction until the V_{ac} has increased to around 3.6 V, which means the emergence of whirling motion considering surface effect requires higher driving forces. For illustrating the process as to when and how the whirling motions starts, the vibration amplitude in Y direction as the V_{ac} varying in the range of (0.6 V – 5.6 V) without surface effect and in (0.5 V – 8.1 V) with surface effect have been calculated, and results are shown in Figures 3a – 3d. The driving frequency is set as $\omega = \omega_0$ in the both cases. It is seen in Figure 3 that vibration in Y not considering surface effect starts from driving voltage of 1.3 V and increases sharply until the voltage point of 2.6 V. It then increases with the driving voltage at a smaller slope. Similar trend is observed for the case of considering surface effect, though the threshold voltage is much higher.

The extensively chaotic motion in silicon nanowire resonator has been reported in [15]. The authors carried a detailed bifurcation analysis and concluded that the nanoscale system can

exhibit distinct chaotic state, where the surface effect has not been considered. Herein, for the high driving voltage V_{ac}, numerical calculations have been conducted to unveil how the surface effect plays its role in determining the nonlinear dynamics. First, the bifurcation diagram has been calculated without surface effect and results are shown in Figure 4a. All the parameters are taken as the same in above except for V_{dc}=25 V. It is shown in Figure 4a that the vibration in Z direction has gone through different states as the V_{ac} is increasing. When V_{ac} is set in (20 V - 21.47 V), the vibration is at a single periodic state. This periodic state has changed into multiple periodic states when V_{ac} increases to the range of (21.47 V - 22.25 V). As the V_{ac} increases further, the vibration in Z direction is back into a single periodic state, and then starts to exhibit multiple periodic states until V_{ac}= 24.5 V. Finally, the vibration has reached to chaotic state. For the purpose of comparison, the bifurcation of vibration in Z direction as the V_{ac} varied in same interval (20 V – 25 V) has been calculated with the surface effect is considered. The result is shown in Figure 4b, it is shown that the vibration when surface effect is considered is basically in multiple periodic states but there are also some parts in which the vibration is at single periodic state. The dynamic performance with surface effect has totally changed under the same driven force. For better illustrating the dynamic process of the system when the V_{ac} is in (20 V– 25 V), the phase portraits have been plotted in Figure 5. It is shown that the system without surface effect goes through a process from periotic to chaotic (Figures 5a – 5e) while the system with surface effect stays in periodic state (Figures 5f – 5h).

Furthermore, We have calculated the Lyapunov exponents as the function of driving voltage V_{ac} of the equation (12). The Lyapunov exponents λ is defined by:

$$\left|\delta Z(t)\right| \approx e^{\lambda t}\left|\delta Z_0\right| \qquad (14)$$

where δz_0 represents initial separation of two trajectories in phase space and $\delta z(t)$ indicates the diverge as the time varying. The result is shown in Figure 6. It should be noted that following relation has been employed in the calculation: $z^{'} = z/h$, $y^{'} = y/h$, $z_1 = z^{'}$, $z_2 = dz^{'}/dt$, $y_1 = y^{'}$, $y_2 = dy^{'}/dt$ and $T = \omega_0 t$. It is shown in Figure 6a that the system without surface effect has the positive max Lyapunov exponent (MLE) λ_1 in the most part of V_{ac} interval (25 V – 30 V), which means that system is vibrating in chaotic state. In the calculation, as there are four first order ordinary differential equations derived from equation (4), there should be four Lyapunov exponents, where $\lambda_1 > \lambda_2 > \lambda_3 > \lambda_4$. In contrast, in Figure 6b, the system with surface effect is still exhibiting periodic vibrations as the λ_1 is negative when driving voltage V_{ac} is in the range of (25 V – 30 V). It is also shown in Figure 6c that λ_1 varies from negative to positive at threshold voltage of around 25 V. In addition, we calculated the λ_1 in a long V_{ac} interval of the system with surface effect, and we found that the system will not be chaotic until the V_{ac} has increased to about 150 V. This to some extent explains the phenomenon that experimental results shown in [23] did not display whirling motions at odds with theoretical prediction [14], in which the surface effect was not considered. In reference [14], it mentioned that with increasing driving voltages the whirling dynamics is unavoidable. Moreover, it has been shown in one of previous publications [20] that the model considering the initial surface stress has led to a more accurate result compared with the one without the surface stress.

Although the elliptic pattern of the whirling motion for device under certain driving conditions has been reported in both the previous articles [14] [15] and this work, detailed analysis of the displacement pattern of the middle point of the doubly clamped SWCNT resonator has not been reported so far. Herein, calculation based on mathematic model described in the previous section has been conducted to unveil the moving trajectory of the central point of

the double clamped SWCNT in *Y-Z* plane, especially when the device is experiencing the whirling and chaotic motions. For the device under very low driving voltages, as there is no *Y* displacement, the displacement trajectory is a straight line in *Z* axis. However as the driving voltage increases to the level at which whirling motion occurs, the displacement pattern will display complex shapes, just like Lissajous curves formed by a pair of parametric equations. According to calculated results, as the driving frequency varies from 1.061 ω_0 to 1.075 ω_0, V_{dc} and V_{ac} are fixed at 0.5 V and 1.6 V respectively, from the Lissajous pattern depicted in Figure 7a, the oscillating frequencies in *Z* and *Y* are the same. It is shown from the results that the whirling trajectories can be categorized into two stable zones, one is centered on the 70° phase deference between *Z*-axis and *Y*-axis oscillations, and the other is centered on the -70° degree phase difference. There is no other intermediate trajectory existing. Increasing the driving voltage to 25 V V_{dc}, while varying V_{ac} from 20.5 V to 21.5 V, Lissajous patterns shown in Figures 7b & 7c indicate that the *Z*-axis oscillation has different frequencies and phases, which is ascribed to multiple periodic states of the oscillations. Further increasing the driving voltage, it is calculated that the oscillator experiences chaotic motions. As a result, the displacement pattern in Y-Z plane displays a filled ellipse shown in Figure 7d, meaning the middle point of the SWCNT could be any position within the outline of the ellipse.

4. Potential Application

A novel application in accelerometer based on the whirling motion of the nanotube has been proposed. While the SWCNT resonator is vibrating, an external acceleration applied in the *Y-Z* plane will change the amplitude of the vibration, which can be detected by either optical or electronic methods. Analysis is conducted to find out the vibrating amplitude change subject to external acceleration/force. In the analysis, the driving voltage V_{dc}=0.5 V and V_{ac}=1.6 V, at

which the whirling motion appears. The driving frequency is set at $1.074\omega_0$. Here we only consider the system without surface effect when $E_s = 0, \tilde{\tau}_{xx} = 0$. The changes of the Z and Y amplitudes have been calculated as the resonator is under a Z-axis acceleration, Y-axis acceleration and Z-Y plane acceleration respectively. The acceleration equivalences f_z and f_y are added to equations (8) and (9), and after conducting the similar derivation procedure as described in previous section, the motion equation is

$$\begin{aligned} &\ddot{z} + \omega_0^2 z + az(z^2 + y^2) + \beta\dot{z} = -2F_0\cos(\omega t) + f_z \\ &\ddot{y} + \omega_0^2 y + ay(z^2 + y^2) + \beta\dot{y} = f_y \end{aligned} \tag{15}$$

where $[f_z, f_y] = \sqrt{2/3}/\rho A \cdot [F_z, F_y]$. The peak amplitudes in Z and Y were calculated as the F_z and F_y increase in the range of [9.91 μN, 57.83 μN]. The results are shown in Figure 8. In Figure 8a, when $F_y = 0$, it is seen that the peak amplitude in Z firstly decreases from 0.24 nm to 0.2 nm and then increases linearly as the acceleration force F_z increases. In Figure 8b, when F_z=0, it is seen that the peak amplitude in Y increases over the whole force range. More calculations have been conducted and the result shown in the Figure 8b demonstrates that linearity of the Y-amplitude versus acceleration force curve has been improved if the surface stress is included. Furthermore, we calculated the case of $F_z \neq 0$ and $F_y \neq 0$ .i.e. when the acceleration force is neither parallel nor perpendicular to the Y- and Z- axis, and the results are shown in Figures 8c and 8d. As expected, the Y component of the force is proportional to the amplitude in Y-axis, and inversely proportional to the amplitude in Z-axis. Similar observation for Z component of the force is shown in the results, except when the F_y is very small, where a notch has been found at F_z = 18.2 μN. In terms of the materials of which accelerometers are made, CNT has much higher Young's modulus (TPa) [8] than silicon (~200 GPa) that is used to make the

microelectromechanical systems (MEMS) accelerometers. Hence high resonant frequencies can be expected using CNT, leading to higher Q (quality) factors. Subsequently the sensitivity will be increased and noise density will be reduced. The disadvantage of the proposed CNT accelerometer is envisaged mainly from aspects of fabrication and signal processing. Quantitative comparison of the above two is hard to make, as the CNT accelerometer is only a conceptual design.

Conclusion: It has been found from the numerical calculations that taking account of very small surface effect E_s = 5.19 Pa (compared with stiffness of the nanotube 5.5 x 10^{12} Pa), the dynamic performances of the SWCNT resonator has changed dramatically. The resonant frequency has increased to nearly twice of the value without surface effect, and the threshold voltage for the whirling motion has increased from 1.4 V to 3.5 V. Detailed analysis of the whirling motions has been conducted, and it is found that the moving trajectories of the central point of the SWCNT resonator follows Lissajous patterns. The nonlinear motions have also changed significantly due to the surface effect from the bifurcation and Lyapunov exponent analysis. The voltage needed to drive the resonator into chaotic motions has increased from 25 V to around 150 V. The reported findings can be used to explain the previous discrepancies between experiments and theories, which will act as a more accurate guidance in designing such resonator devices. A new application in accelerometers using this resonator has been reported and the theoretical analysis is conducted to build the relation between acceleration forces and peak vibrating amplitudes.

Figures:

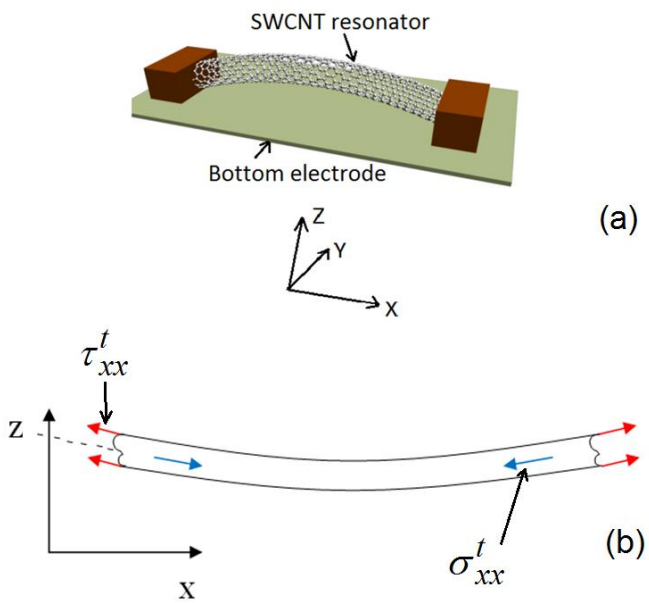

Figure 1a. Schematic diagram of a CNT doubly clamped resonator. Figure 1b, Schematic graph showing the surface stress and the bulk stress.

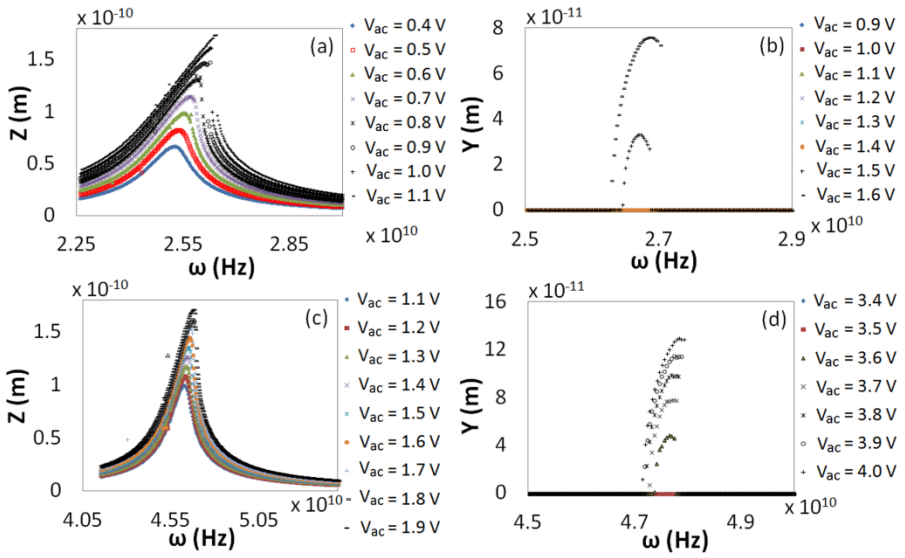

Figure 2. Calculated vibration amplitudes in *Z* and *Y* directions of the system without surface effect under different driving voltage V_{ac} (2a and 2b). Results of the system with surface effect (2c and 2d).

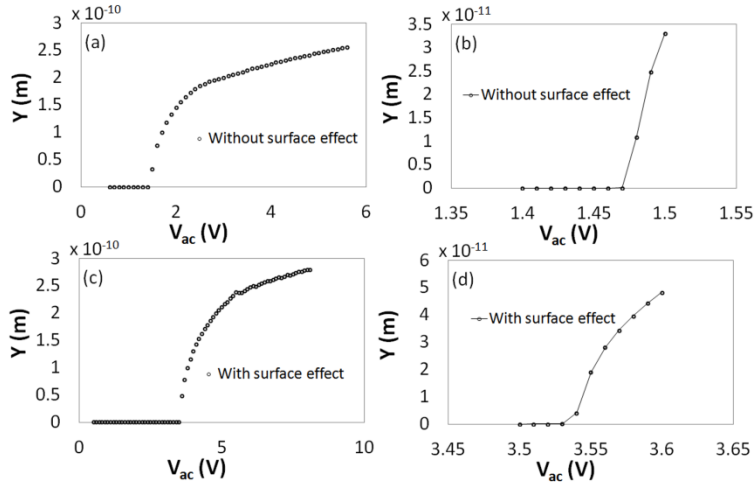

Figure 3. Calculated detailed relation between vibration in Y and applied V_{ac}; without surface effect (3a and 3b); with surface effect (3c and 3d).

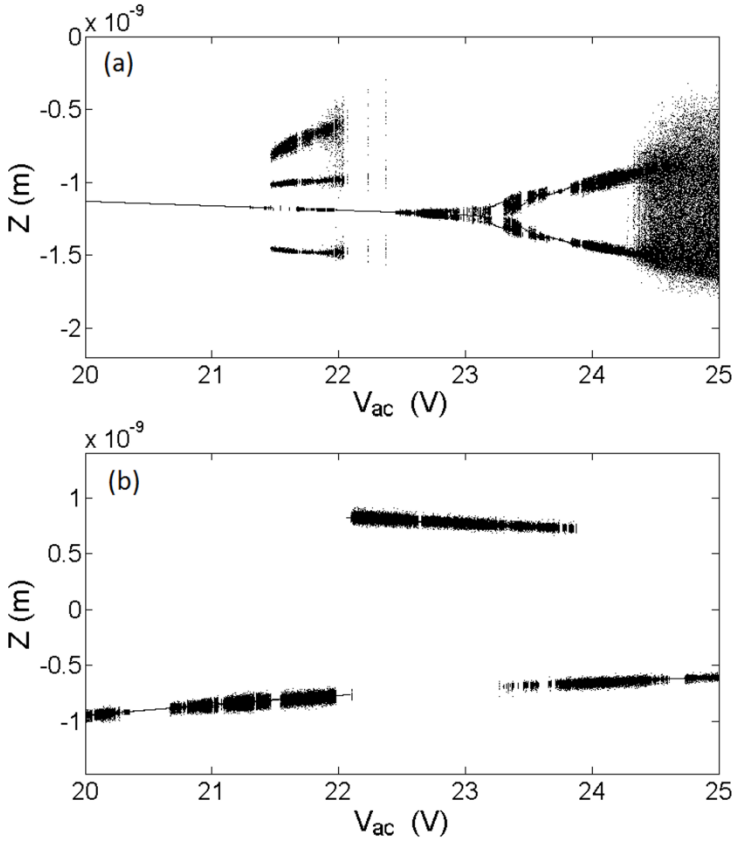

Figure 4. Bifurcation diagram of displacement in *Z* direction of the system withour surface effect in (4a) and with surface effect in (4b) under the same driving voltage V_{ac}.

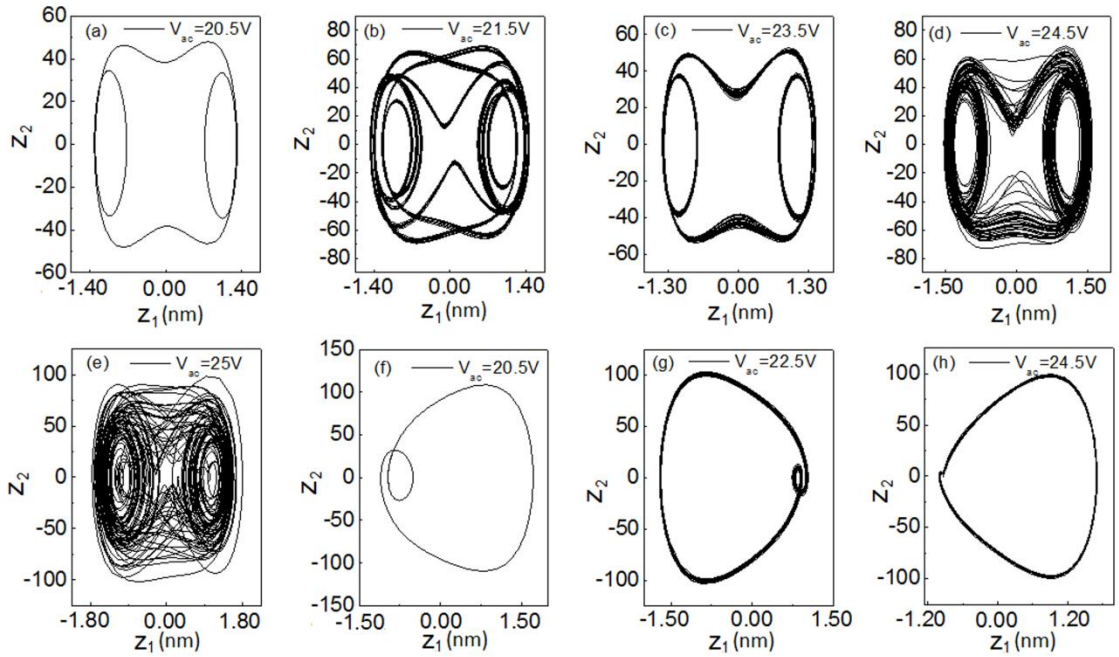

Figure 5. Phase portrait (z_1 vs. z_2)of the system without surface effect in (5a)-(5e) and with surface effect in (5f)-(5h) under the different driving voltages.

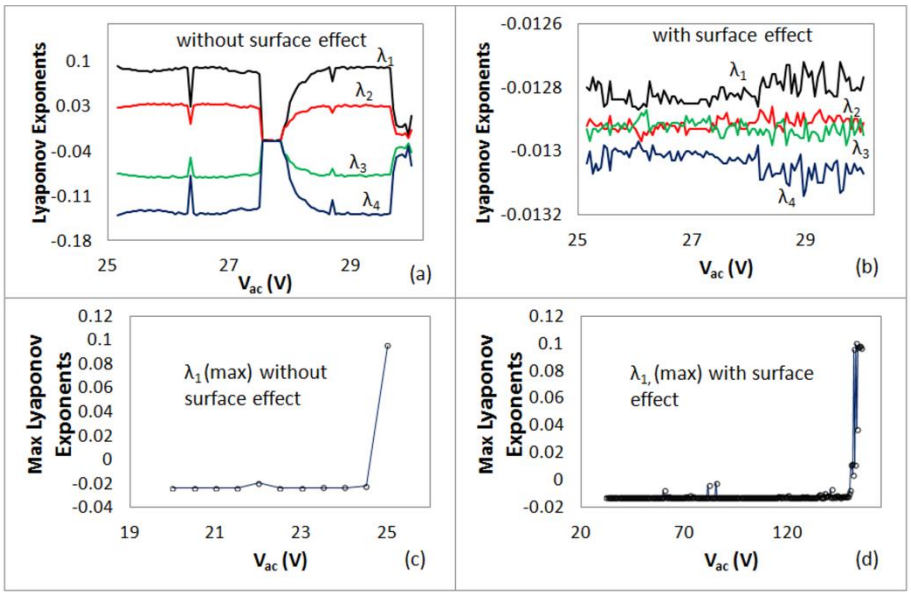

Figure 6. Calculated Lyapunov exponents of the system described by equation (14) without surface effect in (6a) and with surface effect in (6b) driven by V_{ac} in the range of 25 V – 30 V. Transition of calculated max Lyapunov exponents of the same system without surface effect to positive in (6c) and with surface effect in (6d).

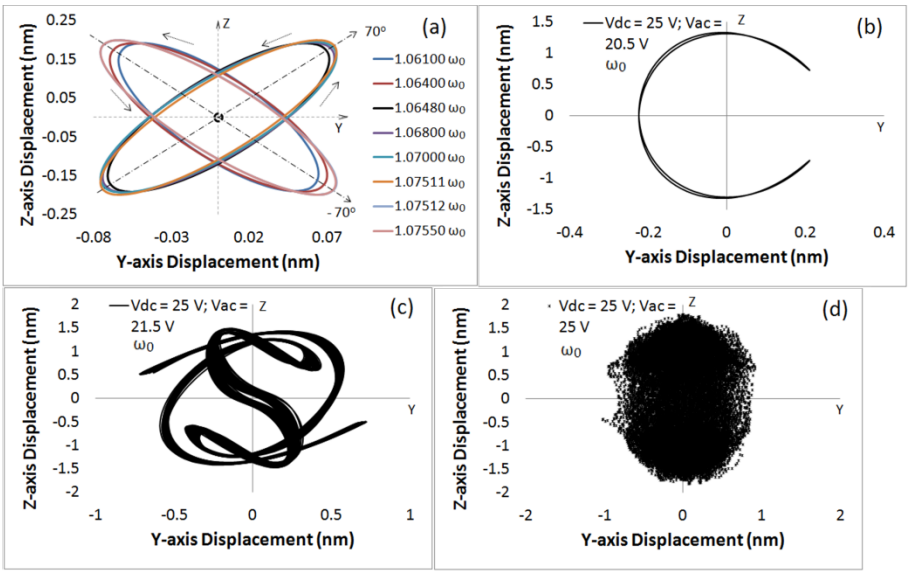

Figure 7. Displacement patterns in Y-Z plane formed by the middle point of the doubly clamped SWCNT resonator under different driving conditions. (a), whiling motions stabilized in two zones; (b), one Lissajous pattern formed by periodic motions in Y and Z with frequency and phase differences; (c) another Lissajous pattern for the Z and Y motions with frequency and phase differences. (d), displacement pattern in Y-Z plane when the device is at chaotic state.

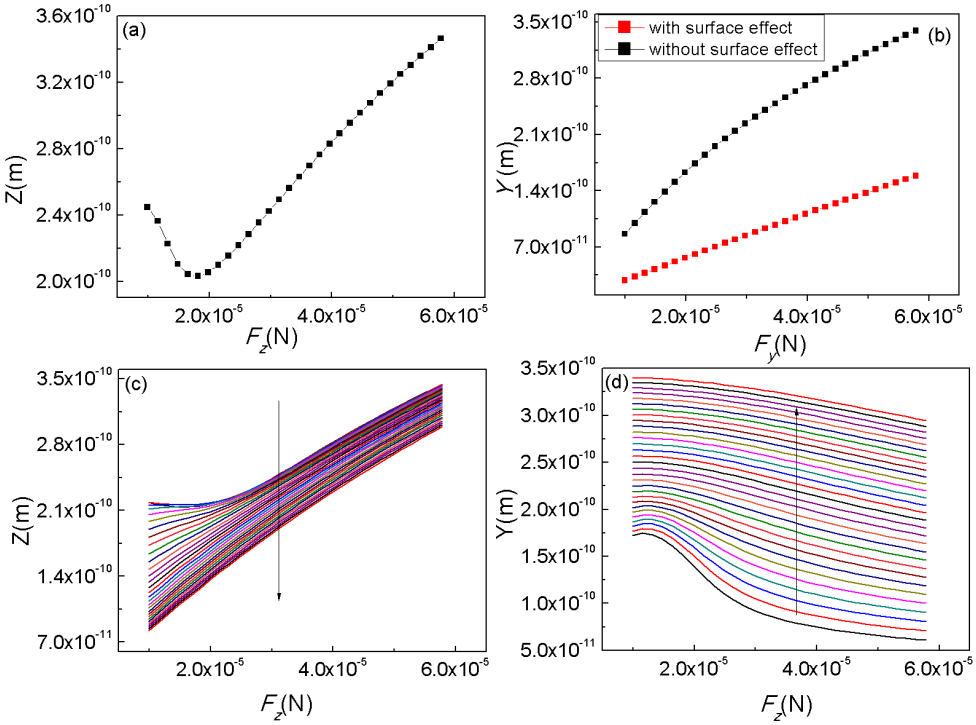

Figure 8. The peak amplitude change in Z and Y directions as the acceleration force varies in the range of [9.91 μN, 57.83 μN]. (a), F_y=0, F_z is varying, results for with and without the surface stress respectively. (b), F_z=0, F_y is varying. (c) & (d), Both F_y and F_z are varying. The arrow in the (c) and (d) indicates the increasing direction of F_y, and the step size is approximately 1.65 μN.

AUTHOR INFORMATION

Corresponding Author

Lijie Li, Multidisciplinary Nanotechnology Centre, College of Engineering, Swansea University, Swansea, SA2 8PP, UK. Email: l.li@swansea.ac.uk; Tel: +44 (0) 1792 606667

Funding Sources

Swansea University and China Scholarship Council.

ACKNOWLEDGMENT

Authors are grateful for the supports of the College of Engineering, Swansea University, and China Scholarship Council.

REFERENCES

1. E. A. Laird , F. Pei , W. Tang , G. A. Steele , and L. P. Kouwenhoven, "A High Quality Factor Carbon Nanotube Mechanical Resonator at 39 GHz," *Nano Letters*, vol. 12, 2012, pp. 193–197.
2. Z. Y. Ning , T. W. Shi , M. Q. Fu , Y. Guo , X. L. Wei , S. Gao , and Q. Chen, "Transversally and Axially Tunable Carbon Nanotube Resonators In Situ Fabricated and Studied Inside a Scanning Electron Microscope," *Nano Letters*, vol. 14, 2014, pp. 1221–1227.
3. A. Croy, D. Midtvedt, A. Isacsson, and J. M. Kinaret, "Nonlinear damping in graphene resonators," *Physical Review B*, vol. 86, 2012, 235435.
4. E. C. Bullard, J. Li, C. R. Lilley, P. Mulvaney, M. L. Roukes, and J. E. Sader, "Dynamic Similarity of Oscillatory Flows Induced by Nanomechanical Resonators," *Physical Review Letters*, vol. 112, 2014, 015501.

5. J. M. Gray, K. A. Bertness, N. A. Sanford, and C. T. Rogers, “Low-frequency noise in gallium nitride nanowire mechanical resonators,” *Applied Physics Letters*, vol. 101, 2012, 233115.
6. H. J. Chen and K. D. Zhu, “Ultrasensitive mass sensing with nonlinear optics in a doubly clamped suspended carbon nanotube resonator,” *Journal of Applied Physics*, vol. 114, 2013, 213101.
7. B. Lassagne, D. Ugnati, and M. Respaud, “Ultrasensitive Magnetometers Based on Carbon-Nanotube Mechanical Resonators,” *Physical Review Letters,* vol. 107, 2011, 130801.
8. M. M. J. Treacy, T. W. Ebbesen, and J. M. Gibson, “Exceptionally high Young's modulus observed for individual carbon nanotubes,” *Nature*, vol. 381, pp. 678-680, Jun 1996.
9. C. C. Wu and Z. Zhong , “Capacitive Spring Softening in Single-Walled Carbon Nanotube Nanoelectromechanical Resonators,” *Nano Letters*, vol. 11, 2011, pp. 1448–1451.
10. C. Li and T. W. Chou, “Mass detection using carbon nanotube-based nanomechanical resonators,” *Applied Physics Letters,* vol. 84, 2004, pp. 5246-5248.
11. T. Rueckes, K. Kim, E. Joselevich, G. Y. Tseng, C. L. Cheung, C. M. Lieber, “Carbon Nanotube-Based Nonvolatile Random Access Memory for Molecular Computing,” *Science*, vol. 289, 2000, pp.94-97.
12. M. D. Dai, C. W. Kim, and K. Eom, “Finite size effect on nanomechanical mass detection: the role of surface elasticity,” *Nanotechnology*, vol. 22, 2011, 265502.
13. R. B. Karabalin, M. C. Cross, and M. L. Roukes, “Nonlinear dynamics and chaos in two coupled nanomechanical resonators,” *Physical Review B*, vol. 79, 2009, 165309.
14. W. G. Conley, A. Raman, C. M. Krousgrill, S. Mohammadi, “Nonlinear and nonplanar dynamics of suspended nanotube and nanowire resonators,” *Nano Letters*, vol. 8, 2008,

pp.1590-1595.

15. Q. Chen, L. Huang, Y. C. Lai, C. Grebogi, and D. Dietz, “Extensively Chaotic Motion in Electrostatically Driven Nanowires and Applications,” *Nano Letters*, vol. 10, 2010, pp. 406-413.
16. H. S. Park, W. Cai, H. D. Espinosa, and H. Huang, “Mechanics of Crystalline Nanowires,” *MRS Bulletin*, vol. 34, 2009, pp.178-183.
17. J. Mei, and L. Li, “Frequency self-tuning of carbon nanotube resonator with application in mass sensors,” *Sensors and Actuators B*, vol. 188, 2013, pp. 661– 668.
18. E. Buks, B. Yurke, “Mass detection with a nonlinear nanomechanical resonator,” *Physical Review E*, vol. 74, 2006, 046619.
19. J. S. Aldridge, A. N. Cleland, “Noise-enabled precision measurements of a duffing nanomechanical resonator,” *Physical Review Letters*, vol. 94, 2005, 156403.
20. F. Song, G. L. Huang, H. S. Park, and X. N. Liu, “A continuum model for the mechanical behavior of nanowires including surface and surface-induced initial stresses,” *International Journal of Solids and Structures*, vol. 48, 2011, pp. 2154-2163
21. L. Meirovitch, *Analytical Methods in Vibrations*, New York: Macmillan, 1967.
22. Y. W. Zhang, T. Z. Yang, J. Zang, and B. Fang, “Terahertz Wave Propagation in a Nanotube Conveying Fluid Taking into Account Surface Effect”, *Materials*, vol. 6, 2013, pp. 2393-2399.
23. V. Sazonova, Y. Yaish, H. Ustunel, D. Roundy, T. A. Arias, P. McEuen, “A tunable carbon nanotube electromechanical oscillator,” *Nature*, vol. 431, 2004, pp. 284-287.